Heterogeneous Catalysis

Subsurface Carbon: A General Feature of Noble Metals

Oriol Piqué[+], Iskra Z. Koleva[+], Francesc Viñes,* Hristiyan A. Aleksandrov,* Georgi N. Vayssilov, and Francesc Illas

Abstract: *Carbon moieties on late transition metals are regarded as poisoning agents in heterogeneous catalysis. Recent studies show the promoting catalytic role of subsurface C atoms in Pd surfaces and their existence in Ni and Pt surfaces. Here energetic and kinetic evidence obtained by accurate simulations on surface and nanoparticle models shows that such subsurface C species are a general issue to consider even in coinage noble-metal systems. Subsurface C is the most stable situation in densely packed (111) surfaces of Cu and Ag, with sinking barriers low enough to be overcome at catalytic working temperatures. Low-coordinated sites at nanoparticle edges and corners further stabilize them, even in Au, with negligible subsurface sinking barriers. The malleability of low-coordinated sites is key in the subsurface C accommodation. The incorporation of C species decreases the electron density of the surrounding metal atoms, thus affecting their chemical and catalytic activity.*

Late transition metals, including coinage (Ni, Cu, Ag, Au) and Pt-group (Pt, Pd, Rh, Ir, Re, Os) metals, are in widespread use as heterogeneous catalysts[1] for many reactions of industrial interest.[2,3] The systems simplicity, triggered by the applications importance, has prompted research aimed at their catalytic activity improvement, desirably coupled with a materials cost reduction. Nanostructuration strategies have been contemplated for that purpose.[4,5] The rational design of novel metal and alloy catalysts, backed up by precise ab initio quantum chemistry calculations on suited catalyst models, has meant as well a great leap forward in the quest for new, improved activity transition metal catalysts.[5,6]

Transition-metal catalysts are typically employed as shape-defined supported metal nanoparticles (NPs), for example, Au NPs on TiO_2 for low temperature carbon monoxide oxidation,[3] or Pd NPs on Al_2O_3 for exhaust gas treatments.[7] The high catalytic performance of such noble metal NPs is inherent to 1) the exposure of facets other than most stable one, and so, chemically more active, and 2) the exhibition of even lower-coordinated sites such as NPs edges and corners, more prone to attach molecules onto;[8] other effects can also play a key role, for example 3) quantum confinement,[8] 4) strong metal–support interactions,[9] 5) nanoparticle flexibility,[10] and 6) nano-polymorphism.[11] Still, the main drawback of such catalysts is that, in the course of the catalysed reaction, these get gradually deactivated over time and use. Besides NP sintering, the origin of this activity loss is the presence of poisoning agents, where carbon excels among others.

Carbon poisoning normally implies C_n moieties, usually generated as a side, undesired product of the on-going catalysed reaction, typically involving organic reagents. At low C coverage, C atoms can strongly adsorb on the catalyst low-coordinated sites, restricting the reagent adsorption upon and/or chemically modifying the very nature of the active sites.[12–14] At high C coverage, monolayers and multilayers of graphene can emerge on top of the metal surface, and even surround and contain metal NPs, structurally fully blocking its active sites.[15,16] However, recent experiments and computational simulations have changed the paradigm of low C content from a poison to a promoter role, as subsurface C in Pd catalysts favours the selective alkyne hydrogenation to olefins,[17] and its presence at low-coordination regions of metal NPs is explained by density functional theory (DFT) based simulations.[14]

Subsurface C has been shown to bias the selectivity of other substitutional or interstitial carbon residues,[18] displaying higher reactivity towards surface O and H adatoms than surface C.[19] The subsurface moieties mediated chemistry is non-exclusive to Pd. Interstitial C is well-known in Ni surfaces and NPs,[16] and recently justified on Pt systems,[20] all belonging to Group 10 of the periodic table. Motivated by these results, a question mark arises: Is such subsurface atom induced chemistry a singularity or a common feature otherwise? In the latter assumption, such effect has been often disregarded, focusing on the vicinal C-perturbing/blocking poisoning picture, which should in fact include the subsurface interaction situation.

Herein we show that the existence of subsurface C is a general feature to be considered. This is confirmed by inspecting its energetic and kinetic stability on most noble metals, namely, Group 11 Cu, Ag, and Au. By means of accurate DFT-based ab initio calculations we give arguments of the competitive, often higher stability of subsurface C compared to surface situations, and its kinetic feasibility by

[*] Prof. O. Piqué,[+] Dr. F. Viñes, Prof. Dr. F. Illas
Departament de Ciència de Materials i Química Física & Institut de Química Teòrica i Computacional (IQTCUB)
Universitat de Barcelona
c/ Martí i Franquès 1, Barcelona 08028 (Spain)
E-mail: francesc.vines@ub.edu

Prof. I. Z. Koleva,[+] Prof. H. A. Aleksandrov, Prof. Dr. G. N. Vayssilov
Faculty of Chemistry and Pharmacy, University of Sofia
1126 Sofia (Bulgaria)
E-mail: haa@chem.uni-sofia.bg

[+] These authors contributed equally to this work.

Supporting information and the ORCID identification number(s) for the author(s) of this article can be found under:
https://doi.org/10.1002/anie.201813037.

overcoming small subsurface sinking energy barriers, with indications of subsurface C being a near-surface entity. DFT results are obtained on periodic supercell slab models suited to describe single-crystal (111) extended surfaces, but also on well-shaped NP models of 79 atoms, a NP size within the scalable regime, and, therefore, representative of larger NPs.[8] For comparison, the surface and subsurface situations are modelled at the (111) surfaces of the other five face-centred cubic (*fcc*) transition metals (Ni, Pd, Pt, Rh, Ir). Further details and definitions are present in the Supporting Information.

The calculated C adsorption (E_{ads}) and absorption (E_{abs}) energies on Cu, Ag, and Au (111) surface slab models for hexagonal close-packed (*hcp*) and *fcc* surface, and tetrahedral subsurface (*tss*) and octahedral subsurface (*oss*) sites, which are the most stable sites, are shown in Figure 1. For Cu, the *hcp* and *fcc* sites have similar stability, 436–440 kJ mol^{-1}, but in the subsurface *oss* site C is more stable by 42 kJ mol^{-1}. For Ag, the surface *fcc* site (E_{ads} of 320 kJ mol^{-1}) is 18 kJ mol^{-1} less stable than the subsurface *oss* site (E_{ads} of 338 kJ mol^{-1}). For Au (111) the surface *fcc* site (E_{ads} of 414 kJ mol^{-1}) is more stable than the subsurface *tss* by 25 kJ mol^{-1}. The main factor for the subsurface stability seems to be a balance between the
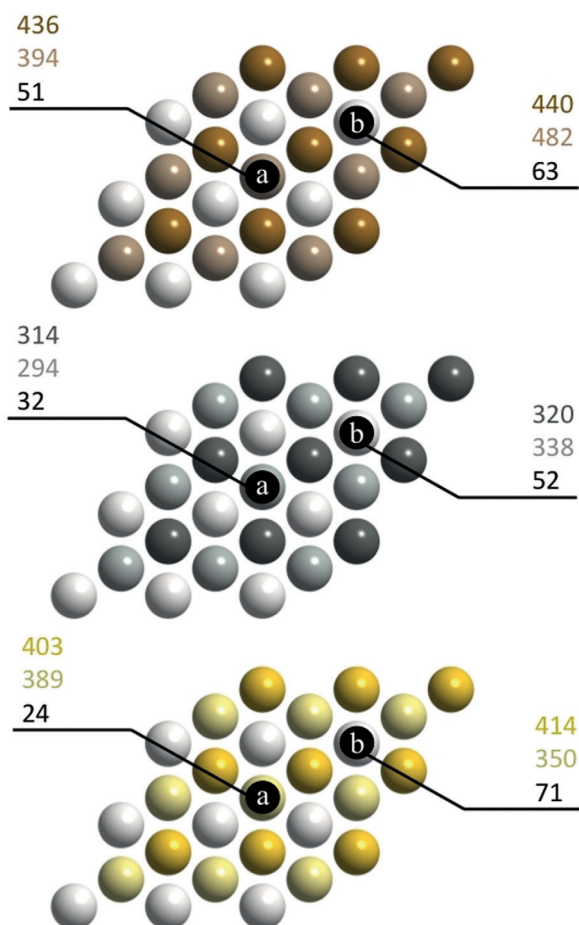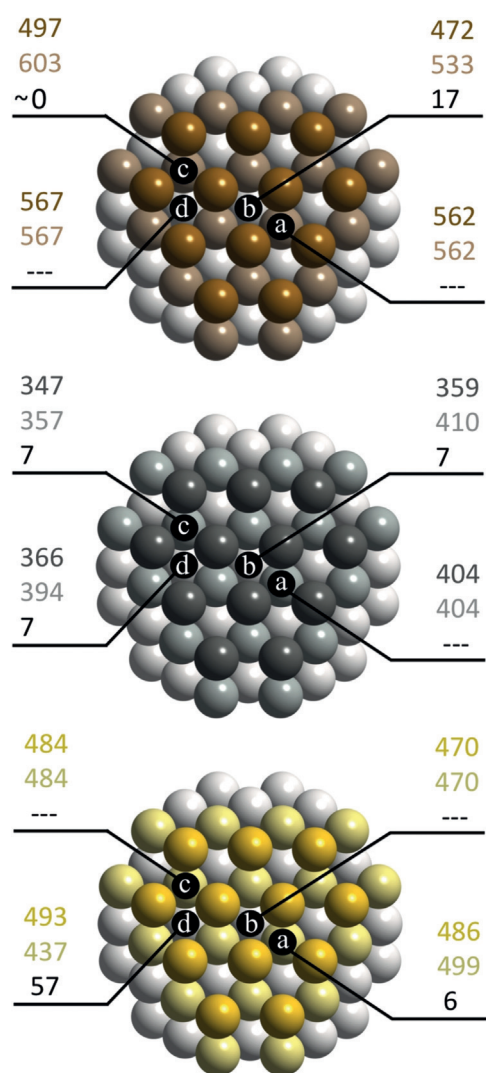
increased C bonding saturation and the subsurface deformation energetic cost to accommodate C atoms within the constrained subsurface space (see the Supporting Information for a discussion of the deformation energies, E_{def}, and Table S1). Moreover, the higher chemical activity of gold compared to silver is explained due to a silver deeper *d*-band centre, as found in equivalent DFT simulations,[21,22] plus a weaker C−Ag coupling, which prevents antibonding states being above Fermi level, and so, destabilizing the C interaction towards Ag.[23,24] Estimates at a full monolayer coverage (Supporting Information, Table S6), show that the surface or subsurface preferential stability prevails, although with reduced E_{ads} and E_{abs}.

A last critical point to tackle is the kinetic hindrance. Subsurface sinking energies displayed in Figure 1 reveal that barriers are within 32 and 63 kJ mol^{-1} for both Cu and Ag (111) surfaces, and, therefore, non-negligible, yet easy to overcome at catalyst working temperatures. For Au (111) the barriers range from 24 to 71 kJ mol^{-1}. The E_{ads}, E_{abs}, and sinking energy barrier values are in line with previous calculations,[20,25] and here well-reproduced for all *fcc* TMs (111) surfaces (Supporting Information, Figure S11). Furthermore, the further penetration of the C atom has been also considered yet discarded (see discussion in the Supporting Information). In general terms Group 11 (Cu, Ag, Au) *fcc* → *oss* sinking barriers are comparable yet higher than Group 10 (Ni, Pd, Pt), despite of the similar stability of the subsurface C. The kinetic hindrance in the former group could explain the lower experimental solubility of C (see discussion in the Supporting Information).

The above results apply for subsurface C suitability on Cu and Ag surfaces under operating conditions. A remaining aspect towards a more holistic picture view is the C interaction in/on lower-coordinated sites, such as edges and corners of metal NPs. This is fully explored on the (111) facets of M$_{79}$ metal NP models (Supporting Information, Figure S2), and E_{ads}, E_{abs}, and subsurface sinking barriers are shown in Figure 2. One immediately detects similarities to extended surfaces, with caveats. Many *fcc/oss* and *hcp/tss* sites featuring both surface and subsurface states on Ag$_{79}$ and Cu$_{79}$ reveal increased E_{ads} and E_{abs} ranging 32–59 kJ mol^{-1} for the adsorption situations and 61–72 kJ mol^{-1} for the absorption situations. For the Au NP the increase of E_{abs} is in general notably higher (87–100 kJ mol^{-1}) than for E_{ads} (79–83 kJ mol^{-1}). Remaining small size effects and the still close proximity to low-coordinated sites can explain the increment of adsorptive situations. In the case of subsurface accommodation, the much larger increment is directly linked to a larger flexibility and deformability of vicinal metal atoms to accommodate and further stabilize the subsurface C moiety. This is clearly highlighted by the deformation and attachment energies balance (Supporting Information, Table S2), where attachment energies can be higher than on the (111) extended surfaces counterparts, by up to 123, 91, and 104 kJ mol^{-1}, for Cu, Ag, and Au NPs, respectively, accompanied by similar deformation energies for surface and subsurface situations. Thus, the low-coordinated sites allow for such deformation, beneficial for the C binding, without compromising the structural energy of the site.

Figure 1. Cu (top), Ag (middle), and Au (bottom) adsorption (E_{ads}, in dark colours) and subsurface absorption energies (E_{abs}, in light colours), in kJ mol^{-1}, on (111) surface a) *hcp* and *tss* sites, respectively, and b) *fcc* and *oss* sites, respectively. Carbon diffusion energy barriers on each site are shown in black.

Figure 2. Cu$_{79}$ (top), Ag$_{79}$ (middle), and Au$_{79}$ (bottom) C adsorption (E_{ads}, in dark colours) and subsurface absorption energies (E_{abs}, in light colours), in kJ mol^{-1}, on diverse (111) facet sites. Carbon diffusion energy barriers on each site are shown in black. Dashed lines are present when in-plane situations are found, that is, adsorption and absorption lead to a common final stable situation (E_{ads} and E_{abs} values are identical).

For the Cu$_{79}$ NP, E_{abs} increases by 209 kJ mol^{-1} with respect the (111) slab model for corner *tss*, which becomes the most stable site for C on Cu$_{79}$. Analogous stabilization of subsurface C is observed on edge *tss* on Au$_{79}$ with an E_{abs} increase of 110 kJ mol^{-1}, with respect to the Au (111) reference. Thus, subsurface C at edge *tss* site becomes the most stable situation in Au$_{79}$, although only 6 kJ mol^{-1} more stable than the edge *fcc* location. On Ag$_{79}$, similarly to Ag (111) surface, the centre *oss* site remains the most stable situation, but only 6 kJ mol^{-1} more stable than the edge *hcp* and *tss* locations. Therefore, low-coordination sites not only preserve the C preference for subsurface in Cu and Ag, but also foster subsurface occupancy even in Au systems. However, at a nearly full coverage situation (Supporting Information, Table S6), the subsurface stability is lost for the NP models, favouring surface situations which can involve the

clustering of C atoms, see the example on Cu$_{79}$ shown in the Supporting Information, Figure S12.

The most prominent feature on all the low-coverage cases is that the energy barriers, E_b, for the subsurface diffusion essentially vanish, and so, there is a kinetic free entrance for C adatoms to the subsurface region at the NPs edge and corner regions. Reduced barriers of essentially zero to 17 kJ mol^{-1} are found to occupy corner *tss* and central *oss* sites in Cu$_{79}$, of 7 kJ mol^{-1} in all situations of Ag$_{79}$ but for the edge *hcp/tss* case, and a reduced barrier of only 6 kJ mol^{-1} for the entrance towards the edge *hcp* site in Au$_{79}$. This energy barrier lowering located at under-coordinated sites was also earlier found for Pd NPs.[14] Moreover, it has been found that low-coordination sites geometrically approach the surface and subsurface minima of the ad/absorbed C atom (see discussion in Supporting Information and Figures S3 and S4).

A further question is whether such subsurface C occupancy would be thermodynamically driven. To this end, phase diagrams have been acquired for all *fcc* TMs (111) surfaces, considering the turning conditions of pristine surfaces to become early C-containing, either on surface (C^{sur}) or in subsurface (C$_{sub}$). The details on phase-diagram construction, equalling the chemical potential of C, μ(C), to be half of that of acetylene (C$_2$H$_2$) minus hydrogen (H$_2$) molecular gases,[26] thus emulating alkyne hydrogenation conditions,[17] are given in the Supporting Information. The phase diagrams in the Supporting Information, Figure S9, show that, at regular catalytic temperature working conditions, C adatoms would be thermodynamically stable on Rh, Ir, and Pt (111) surfaces, subsurface on Ni and Pd (111) surfaces, and thermodynamically unstable on Cu, Ag, and Au (111) surfaces. This highlights that, on the latter, the isolated C adatom existence would be only dynamically and/or kinetically prompted, and to be considered only on the course of the reaction, even though the final state of such C moieties would be aggregate in graphite or amorphous carbon phases. However, note that the thermodynamic stability is reachable on low-coordinated sites of the Cu$_{79}$ NP (Supporting Information, Figure S10). In any case, the ex situ subsurface C detection on Cu, Ag, and Au regular surfaces does not seem feasible, and a challenging task in situ (for example, see the discussion based on ambient pressure X-ray photoemission spectroscopy (APXPS)[27] in the Supporting Information), where indirect approaches through modified surface activity or site specific surface science techniques seem more feasible for the detection of subsurface C species in noble-metal systems.

Furthermore, to estimate the changes in the electronic structure of the three metals upon adsorption or absorption of C, we calculated the difference between the 3s core levels of metal centres around C and the corresponding centres in the pristine models before C insertion (Table 1; Supporting Information, Table S6). In all cases, there is a stabilization of the metal core level energies, suggesting a decrease of the electron density, and hence, a partial positive charge on those metal atoms. The core levels of surface atoms bound to C on Cu and Au (111) surfaces are stabilized by 0.63–0.94 and 0.65–0.89 eV, respectively, while for the Ag (111) surface this interval is 0.27–0.55 eV. For the subsurface atoms this stabilization appears to be smaller, for example, for the *oss*

Table 1: Shifts (in eV) of the 3s core levels (positive values correspond to stabilization) and of the *d*-band centres ε_d of the metal atoms bound to the carbon with respect to the corresponding metal atoms in the pristine (111) slab model.

		3s Core-level shifts			ε_d		
		Cu	Ag	Au	Cu	Ag	Au
fcc		0.94	0.55	0.89	−0.90	−0.40	−0.79
oss	Surf	0.63	0.27	0.65	−0.64	−0.24	−0.63
	Subs	0.46	0.08	0.13	−0.47	−0.07	−0.13
hcp		0.96	0.56	0.88	−0.92	−0.41	−0.79
tss	Surf	0.65	0.30	0.69	−0.65	−0.25	−0.66
	Subs	0.61	0.18	0.54	−0.60	−0.11	−0.43

position of the Au slab the energy decrease is 0.65 and 0.13 eV for surface and subsurface Au atoms, respectively. Along the same line, the metal reactivity change is measured by the *d*-band centre shift of the metal atoms bound with the C atom with respect to the same atomic values on the corresponding pristine model. The obtained values reveal the same trend as the 3s core levels (Table 1; Supporting Information, Table S6). For instance, for Cu, Ag, and Au (111) surfaces with C at *fcc* or *hcp* positions, the shift of *d*-band centres to lower energies is 0.90/0.92, 0.40/0.41, and 0.79/0.79 eV, thus making the sites a priori less chemically active. The values for the slab and NP models are comparable. Again, the effect of subsurface C is weaker than that of the C atoms on the metal surface.

The density of states (DOS) difference plots for 5*d* states of Au metal centres bound to C at *oss* position of the Au (111) and at *hcp* edge of the NP are shown with solid lines in Figures 3a and b, respectively (the DOS plots for Cu and Ag are provided in the Supporting Information, Figures S5 and S6). For both slab and NP models there is an increase of DOS in the −7.5 to −4.0 eV region upon C absorption; while in the −3 to −1 eV region, closer to the Fermi level, a strong depletion of DOS is observed. This picture is in agreement with the stabilization of these metal centres, concluded from the analysis of the previous characteristics. Interestingly, when considering these metal-atom DOS plots in the same geometry while removing the C atom (see the dashed lines in Figure 3a,b), the opposite trend is observed; 5*d* DOS increases strongly close to the Fermi level and decreases at lower energies. Finally, in Figures 3c–f the charge density difference for some of the C-containing Au models is visualized (see also the Supporting Information, Figures S7 and S8 for the other C positions and metals). These figures confirm that there is a depletion of electron density from the metal centres around C (blue

regions) and a rearrangement of electron density at those centres, likely due to a rehybridization of their frontier orbitals.

In summary, the present findings provide compelling energetic plus kinetic evidence that subsurface C species are to be considered in coinage metal systems, from extended surfaces to low-coordinated sites present in metallic NPs, under working catalytic temperature conditions. In the case of low-coordinated sites such as NPs edges and corners, subsurface positions are the most stable situation at low C concentrations, even in gold, to the point of subsurface C being a thermodynamically viable phase in Cu low-coordinated sites. On extended (111) facets/surfaces, subsurface C is dynamically and kinetically envisaged on Cu and Ag systems. These results broaden the subsurface C chemistry, so as to be considered a general aspect of late transition metal systems.
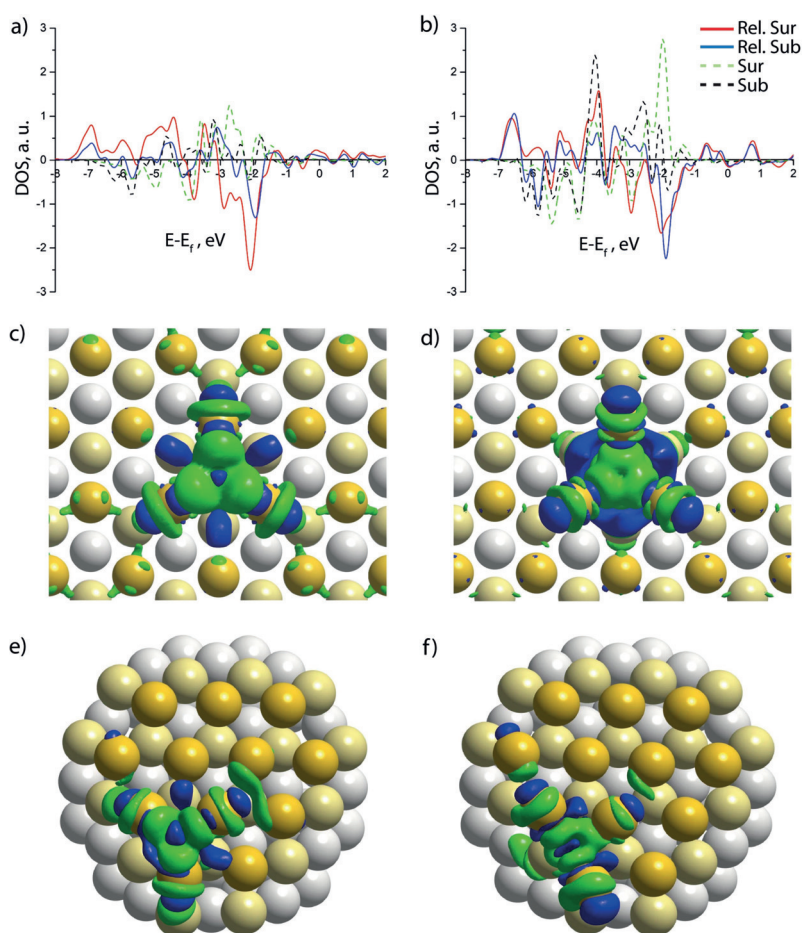
Figure 3. Difference in the density of states plots of Au 5*d* states for metal centres bound to C and corresponding Au atoms in a) the pristine model for C in *oss* position on Au (111) surface and b) C in *hcp* edge position on Au₇₉ NP. Red solid line for surface Au atoms; blue solid line for subsurface Au atoms; dashed lines belong to difference between single point calculations for the corresponding structures after removal of C and the corresponding atoms in the pristine optimized structure: green dashed line belongs to surface Au atoms; black to subsurface Au atoms. The plots are normalized with respect to the number of gold atoms around the carbon. c)–f) Charge density difference for surface *fcc* (c) and subsurface *oss* (d) positions of C on Au(111) slab model; surface *fcc* edge (e) and *oss* edge (f) positions of C on Au NP: green regions indicate the increase of the electron density due to C addition, and blue regions the electron density depletion.

The malleability of low-coordinated sites at surfaces, edges, and corners appears to be the key aspect in the subsurface site C accommodation. Furthermore, this aspect does explain the easy sinking of surface C species to near surface situations, with low diffusion energy barriers, from almost vanishing at NPs edges and corners. The experimental in situ identification of such C species is challenging, although its presence may explain previously observed peculiar surface chemical activities of coinage metals with C impurities, and, furthermore, introduces itself as an aspect to be regarded in the future when studying heterogeneously catalysed processes by transition metal systems. The analysis of electronic structure changes in the C surrounding metal atoms reveals electron deficiency at those centres, indicating a partial positive charge that will affect their chemical and catalytic properties.

Conflict of interest

The authors declare no conflict of interest.

[1] J. Greeley, J. K. Nørskov, M. Mavrikakis, *Annu. Rev. Phys. Chem.* **2002**, *53*, 319.

[2] A. J. Medford, A. Vojvodic, J. S. Hummelshøj, J. Voss, F. Abild-Pedersen, F. Studt, T. Bligaard, A. Nilsson, J. K. Nørskov, *J. Catal.* **2015**, *328*, 36.

[3] M. Haruta, S. Tsubota, T. Kobayashi, H. Kageyama, M. J. Genet, B. Delmon, *J. Catal.* **1993**, *144*, 175.

[4] F. Zaera, *ChemSusChem* **2013**, *6*, 1797.

[5] J. K. Nørskov, T. Bligaard, J. Rossmeisl, C. H. Christensen, *Nat. Chem.* **2009**, *1*, 37.

[6] S. M. Kozlov, G. Kovács, R. Ferrando, K. M. Neyman, *Chem. Sci.* **2015**, *6*, 3868.

[7] F. Viñes, A. Desikusumastuti, T. Staudt, A. Görling, J. Libuda, K. M. Neyman, *J. Phys. Chem. C* **2008**, *112*, 16539.

[8] F. Viñes, J. R. B. Gomes, F. Illas, *Chem. Soc. Rev.* **2014**, *43*, 4922.

[9] S. J. Tauster, *Acc. Chem. Res.* **1987**, *20*, 389.

[10] H. A. Aleksandrov, S. M. Kozlov, S. Schauermann, G. N. Vayssilov, K. M. Neyman, *Angew. Chem. Int. Ed.* **2014**, *53*, 13371; *Angew. Chem.* **2014**, *126*, 13589.

[11] B. K. Min, C. M. Friend, *Chem. Rev.* **2007**, *107*, 2709.

[12] S. M. Davis, G. A. Somorjai, *The Chemical Physics of Solid Surfaces and Heterogeneous Catalysis*, Elsevier, Amsterdam, The Netherlands, **1983**.

[13] S. Vajda, M. J. Pellin, J. P. Greeley, C. L. Marshall, L. A. Curtiss, G. A. Ballentine, J. W. Elam, S. Catillon-Mucherie, P. C. Redfern, F. Mehmood, P. Zapol, *Nat. Mater.* **2009**, *8*, 213.

[14] F. Viñes, C. Loschen, F. Illas, K. M. Neyman, *J. Catal.* **2009**, *266*, 59.

[15] S. K. Sengar, B. R. Mehta, R. Kumar, V. Singh, *Sci. Rep.* **2013**, *3*, 2814.

[16] H. A. Aleksandrov, N. Pegios, R. Palkovits, K. Simeonov, G. N. Vayssilov, *Catal. Sci. Technol.* **2017**, *7*, 3339.

[17] D. Teschner, J. Borsodi, A. Wootsch, Z. Révay, M. Hävecker, A. Knop-Gericke, S. D. Jackson, R. Schlögl, *Science* **2008**, *320*, 86.

[18] A. Rinaldi, J.-P. Tessonnier, M. E. Schuster, R. Blume, F. Girgsdies, Q. Zhang, T. Jacob, S. B. Abd Hamid, D. S. Su, R. Schlögl, *Angew. Chem. Int. Ed.* **2011**, *50*, 3313; *Angew. Chem.* **2011**, *123*, 3371.

[19] M. Maciejewski, A. Baiker, *Pure Appl. Chem.* **1995**, *67*, 1879.

[20] P. Janthon, F. Viñes, J. Sirijaraensre, J. Limtrakul, F. Illas, *Catal. Sci. Technol.* **2017**, *7*, 807.

[21] Y. Santiago-Rodríguez, J. A. Herron, M. C. Curet-Arana, M. Mavrikakis, *Surf. Sci.* **2014**, *627*, 57.

[22] B. W. J. Chen, D. Kirvassilis, Y. Bai, M. Mavrikakis, *J. Phys. Chem. C* **2018**, https://doi.org/10.1021/acs.jpcc.7b11629.

[23] B. Hammer, J. K. Nørskov, *Adv. Catal.* **2000**, *45*, 71.

[24] A. Notario-Estévez, S. M. Kozlov, F. Viñes, F. Illas, *Chem. Commun.* **2015**, *51*, 5602.

[25] S. P. Liu, M. Zhao, W. Gao, Q. Jiang, *ChemSusChem* **2017**, *10*, 387–393.

[26] D. Teschner, Z. Révay, J. Borsodi, M. Hävecker, A. Knop-Gericke, R. Schlögl, D. Milroy, S. D. Jackson, D. Torres, P. Sautet, *Angew. Chem. Int. Ed.* **2008**, *47*, 9274–9278; *Angew. Chem.* **2008**, *120*, 9414–9418.

[27] M. Favaro, H. Xiao, T. Cheng, W. A. Goddard III, J. Yano, E. J. Crumlin, *Proc. Natl. Acad. Sci. USA* **2017**, *114*, 6706.